The Boomerang Nebula – The Coldest Region of the Universe?

Raghvendra Sahai

Jet Propulsion Laboratory MS 183-900, California Institute of Technology, Pasadena 91109, USA

Lars–Åke Nyman

European Southern Observatory, Casilla 19001, Santiago 19, Chile, and Onsala Space Observatory, S-439 92 Onsala, Sweden

Received ____________________; accepted ____________________

Submitted to Astrophysical Journal (Letters)

1. Introduction

The transition of Asymptotic Giant Branch (AGB) stars into planetary nebulae occurs over a very short period ($\sim$ 1000 yrs) (e.g. Schönberner 1990). Objects in this evolutionary phase, called protoplanetary nebulae (PPNe), are therefore, rare objects. Consequently, the protoplanetary phase of stellar evolution is very poorly understood, but probably holds the key to the long--standing puzzle of how red giant stars anti their surrounding mass--loss envelopes (which are largely round) transform themselves into the dazzling variety of asymmetric morphologies seen in planetary nebulae (e.g. Schwarz, Corradi, & Melnick 1992). The Boomerang Nebula (e.g. Wegner & Glass 1979, Taylor & Scarrot 1980) with its distinctly bipolar morphology similar to that of the prototype PPN, CRL2688 (e.g. Latter et al. 1993) is an important member of the class of known PPNe. In such nebulae, the central star is hidden behind a dusty, flattened cocoon seen roughly edge-on, allowing starlight to escape preferentially along the polar directions and illuminate a pair of reflection nebulosities above and below the cocoon. Almost, all of the nebular material surrounding the obscured central star in PPNe consists of cold molecular gas, ideally probed through observations of millimeter--wave rotational lines. In this Letter, we report such observations of the Boomerang Nebula which show it to be a unique object, consisting of an ultra--cold and extremely massive molecular envelope, expanding at a very high speed. The extreme physical characteristics of the Boomerang Nebula reported here have never been seen before in any AGB or post- AGB object, and should spur new theoretical and observational efforts to understand the nature of the mass- loss processes occurring during late stellar evolution.

2. Observations and results

Millimeter-wave CO observations of the Boomerang Nebula were made using the 15111 SEST (Swedish-ESO Submillimeter Telescope), situated on La Sills, Chile. The data were noted from absorption lines seen in optical spectra of the nebula (Neckel et al. 1987). The central emission feature in the spectra indicate a second outflow with a smaller expansion velocity (35 km s⁻¹). In the CO J = **2--1** transition, only the central emission feature is seen there are no absorption features. We have also mapped the nebula in the CO J = *1-0* transition in order to determine its spatial structure and extent. Maps of the CO (l-O) features in different velocity intervals show that the distribution of molecular gas in the nebula is largely roughly spherical (Fig. 2), although there are small differences between the sloping red and blue wings of the CO $J = 1–0$ absorption profile. A comparison of the absorption line intensities measured on and off the source-center shows that the wide CO (l-O) absorption feature is spatially extended w.r.t the 45" beam. A similar exercise for the integrated intensity of the central "bump" feature ($-45 < V_{LSR} < 25 \mathrm{kms}^{-1}$), measured as an "excess" over the underlying absorption, shows that it is spatially unresolved. In contrast to the CO, an optical V–band image taken with the New Technology Telescope (NTT) at ESO (Fig. 2d) shows a clearly bipolar morphology.

EDITOR: PLACE FIGURE 2 HERE.

We have measured a 9 mK upper limit (3σ) on continuum emission at 89.2 and 145.6 GHz towards the Boomerang, which is much smaller than the negative temperatures seen in the CO and ^{13}CO $J = 1-0$ spectra, so these must result from absorption of the microwave background, requiring the excitation temperature (T_{ex}) to be less than 2.8K (T_{bb}). This is because the antenna temperature measured through our '(on source - off source" observations is an excess over T_{bb}, and is equal to: $I(ON) - I(OFF)$, with $I(ON) = (\lambda^2/2k)[B(T_{bb})$ e-T $+ B(T_{ex})$ $(1 - e^{-\tau})]$, and $I(OFF) = (\lambda^2/2k) B(T_{bb})$, where τ is the optical depth, and B is the Planck black-body function. Hence if $T_{ex} < T_{bb}$, and $\tau >> 1$, then $I(ON) - I(OFF) = (\lambda^2/2k)[B(T_{ex}) - B(T_{bb})] < 0$. Using self-consistent modelling of radiative transfer, excitation, and energy balance, Sahai (1990) predicted

R_2 = *33" (7.2 x* 10^{17} cm), and $V_{\rm exp}(2)$ = *164* km s^{-1}. In shell 1, $T_{\rm kin}$ >2.8 *K,* and $T_{\rm ex}(1\text{-}0)$ as well as $T_{\rm ex}(2\text{-}1)$ are both >2.8 K. In shell 2 $(R_{1,o} < r < R_2)$, $T_{\rm kin}$ <2.8 K, 2%,(1-0) <2.8 K, $\tau(1\text{-}0) > 1$, $T_{\rm ex}(2\text{-}1)$ = 2.8 K and $\tau(2\text{-}1) < 1$. The local maximum at the center of the CO and ^{13}CO(1–0) lines is due to emission from shell 1 superimposed on absorption due to shell 2. The assumption of sphericity is the simplest one for shell 1, which is unresolved, and reasonable for shell 2, since the contours of absorption intensity shown in Fig. 2 show only mild departures from circularity. Radiation from any point in shell 1 can pass unaffected through line-of-sight material in shell 2 due to the doppler-shift induced by the large relative velocities between points in the two shells, simplifying the treatment of radiative transfer. Details of the radiative transfer and statistical equilibrium computation are essentially similar to that for a single spherical shell, as described in Sahai (1987). The model emergent intensity distribution for each transition has been convolved with gaussian beams of the appropriate sizes to produce spectra which can be directly compared with the observations. The CO/H_2 (number) abundance ratio is found to be about 10^{-3} in the outer shell; the same value has been adopted for the inner shell. Assuming the kinetic temperature to be $T_{\rm kin}(r) = T_o\,(r/6'')^{\beta}$ where β = -1.33, as expected for an envelope where adiabatic cooling dominates all thermodynamic processes, we find T_o = 4 and 2.8 K in shell 1 and 2. The required mass-loss rates are $\geq 10^{-4}\,M_\odot\,yr^{-1}$ in shell 1 and 1.3 x $10^{-3}\,M_\odot\,yr^{-1}$ in shell 2. Fig. 3 shows the model spectra – - these fit the data (Fig. 1) reasonably well. Our model also reproduces (to within $\sim$15%) the decrease in CO (l--O) absorption intensity as seen in the mapping data, providing an additional check on the sizes of shells 1 and 2.

EDITOR: PLACE FIGURE 3 HERE.

The inner radius of shell 1 is sensitively constrained by the ratio of the peak CO (2-1) emission intensity to the amplitude of the central bump in the CO (1- O) spectrum. The of the radial velocity structure, We now estimate the range of physical parameters that can produce good fits to the data. The derived value of dM/dt (1.3 x $10^{-3}\,M_\odot\,yr^{-1}$) in shell 2 is very large, even when compared to the. highest mass- loss rates seen so far [e.g. using CO spectra, mass-loss rates of $\sim 10^{-4}\,M_\odot\,yr^{-1}$ have been found in the extended envelopes of CRL2688 (Truong-Bach et al 1990) and NGC7027 (Jaminet et al 1991)]. However, the former is quite robust (uncertain by a factor < 1.5), since it is bracketed at the lower end by the requirement that collisional excitation be effective in driving T_{ex}(1-0) sufficiently below 2.8 K (to produce the observed CO (1–0) absorption), and at the upper end by the requirement that the (2–1) optical depth remain smaller than unity (to prevent (2--1) absorption). The CO abundance, $f(CO)$, is constrained by the requirement that $f(CO)$ x dM/dt must be large enough to make the (1-0) line sufficiently optically thick in shell 2 in order to prevent the microwave background from leaking in and raising T_{ex} (1–0) towards 2.8 K, and is about the maximum value expected for a carbon-rich AGB envelope (1.3 x 10^{-3}, if the O/H abundance is solar, and O is fully associated into CO). We have used a source distance of 1500 pc. With $D = 2500$ pc as suggested by BB, even with both $f(CO)$ and dM/dt as high as $10^{-3}\,M_\odot\,yr^{-1}$, the CO(1–0) absorption signal is too weak (–0.08 K). Merely increasing the source size does not increase the absorption signal because beyond a certain radius (7 x 10^{17} cm), the CO(1- 0) becomes optically thin, and $T_{ex}(1\text{–}0)$ becomes 2.8 K. If $D > 1500$ pc, we require $dM/dt > 10^{-3}\,M_\odot\,yr^{-1}$ to fit the data. For $D < 1500$ pc, acceptable fits can be obtained by scaling the nebula to keep the angular distribution of kinetic temperature and tangential optical depth the same (requiring dM/dt to scale linearly with D), however for $D \leq 1000$ pc, the stellar luminosity $L_* \leq 120\,L_\odot$, unacceptably low for the central star of a pre -planetary nebula. The physical properties of shell 1 are more uncertain than those of shell 2. Keeping the CO abundance at the same value as that found for shell 2, the observed amplitudes of the emission bumps in the (2- 1) and (1-0) CO spectra require $dM/dt \gtrsim 10^{-4}\,M_\odot\,yr^{-1}$. If shell 1 is not spherically mass-loss rate, and a relatively low luminosity central star (Sahai et al. 1994). As pointed out by Sahai et al. (1994), for both M1–16 and the Boomerang, the mechanical wind momentum (dM/dt x V_{exp}) far exceeds the total radiative momentum (L_*/c), making radiation-pressure driven mass loss mechanisms untenable. Using the luminosity of the Boomerang central star estimated by BB scaled to our adopted distance of 1500 pc (300 $L_\odot$), the ratio of $dM/dt \times V_{exp}$ to L_*/c comes out to be 4×10^4. The physical mechanism responsible for driving the 164 km s^{-1} outflow in the Boomerang is thus unknown. The total amount of matter in the Boomerang Nebula is prodigious, with at least 1.9 $M_\odot$ in the outer shell alone, giving a lower limit of about 2.6 $M_\odot$ for the main n-sequence progenitor of the Boomerang (since white dwarf masses lie in a relatively narrow range of 0.5--0.6 $M_\odot$).

The spatio-kinematic structure of the Boomerang (an inner shell with a small expansion velocity, and an outer shell with a very large expansion velocity) is unique among AGB/post–AGB objects. If we assume that the expansion velocity of the material in each shell does not change substantially after a short period of initial acceleration, we find that the expansion time-scales of the inner and outer shell — 1250 and 1450 yr, respectively — are comparable. We think that it is rather improbable for a single star to simultaneously produce two massive outflows with such different expansion velocities via the same physical mechanism, and suggest that the inner shell has a different origin than the outer one. A possible mechanism is the ejection of a common envelope (CE) by a central binary star (Livio 1993), with the ejected material being largely confined to low latitudes (i.e in and near the plane of the nebular waist). The bipolar shape of the optical reflection nebula then results from starlight escaping preferentially from the less dense polar regions of the inner shell and anisotropically illuminating the extended, spherical nebula (i.e. shell 2). This viewpoint is in marked contrast to the traditional one in which the extended nebula is intrinsically anisotropic, with the density decreasing monotonically with latitude from the equatorial plane (orthogonal to the long axis of the nebula) to the polar axis (Morris

REFERENCES

Bujarrabal, V. & Bachiller, R. 1991, A&A, 242, 247

Jaminet, P. A., Danchi, W. C., Sutton, E. C., Russell, A. P. G., Sandell, G., Bieging, J. H., & Wilner, D.A. 1991, ApJ, 380, 461

Jura, M., Kahane, C., and Omont, A. 1988, A&A, 201, 80

Knapp, G.R. & Chang, K.M. 1985, ApJ, 293, 281

Lambert, D. L., Gustafsson, B., Eriksson, K., & Hinkle, K.H. 1986, ApJS, 62, 373

Latter, W. B., Hera, J. L., Kelly, D. M., Deutsch, L. K., & Maloney, P.R. 1993, AJ, 106, 260

Livio, M. 1993, in IAU Symp. 155, Planetary Nebulae, eds. R. Weinberger & A. Acker, Kluwer, 279

Morris, M. 1981, ApJ, 249, 572

Neckel, T., Staude, H. J., Sarcander, M., & Birkle, K. 1987, A&A, 175, 231

Sahai, R. 1987, ApJ, 318, 809

Sahai, R. 1990, ApJ, 362, 652

Sahai, R., Wootten, A., Schwarz, H. E., & Wild, W. 1994, ApJ, 428, 237

Sahai, R., Trauger, J. T., Evans, R.W. & the WFPC2 IDT, 1995, BAAS, 27, 1344

Sahai, R., Trauger, J. T., Watson, A. et al 1997, ApJ, (submitted)

Schwarz, H. E., Corradi, R.L.M. & Melnick, J. 1992, A&AS, 96, 23

Schönberner, D. 1990, in From Miras to Planetary Nebulae - Which Path for Stellar Evolution?, eds. M.O. Mennessier & A. Omont (Editions Frontières), 355

Fig. 1--- CO (1- O), ^{13}CO (l--O), and CO (2- 1) spectra taken towards the center of the Boomerang Nebula ($\alpha_{1950} = 12^h41^m54^s.2, \delta_{1950} = -54°14'47''$) using the 15m Swedish-ESO Submillimetre Telescope The ^{13}CO (1-O) spectrum has been scaled by a factor 5, and a constant (0.2 K) has been subtracted to shift it away from the CO (l--O) spectrum for clarity. The LSR radial velocity of the central star (– 10 km s^{-1}), measured from the center of symmetry of the CO J = *2–1* line, is marked in the spectra. The negative temperatures seen in the J = *1–0* spectra result from absorption of the microwave background radiation by ultra-cold gas in the nebula.

Fig. 2.— Contour maps of the CO(1–0) features in different velocity intervals, and an optical image taken with the NTT at ESO. The CO data were taken every 22", half the telescope bearnwidth. Dots mark observed positions. The spatial scale, shown only in (c), is the same for all panels. Panel (a) shows the intensity integrated over the full velocity extent of the CO feature (-180 to 156 km s-l). Contours are from -40 to -4 in steps of 4 K km s-l. Panels (b) and (c) show the intensity integrated over velocity sub-intervals in the blue (-180 to -43 ktn s^{-1}) and red wings (23 to 156 km s^{-1}) of the feature, showing regions of the high-velocity outflow moving towards (b), and away from us (c). Contours are in steps of -2 K km s^{-1} starting at -2 K km s^{-1}. The 1 σ noise in the CO maps is $\sim$ 0.7 K km s¯1. Panel (d) shows a logarithmically-stretched, uncalibrated optical V-band image in inverted grey–scale. Since the CO maps show only small departures from circular symmetry, we assume a spherical distribution of molecular gas in the nebula for modelling purposes.

Fig. 3.-– Spectra from a two- shell model for the Boomerang Nebula that fit the CO observations reasonably well. The LSR radial velocity of the central star (– 10 km s^{-1}) is marked in the spectra. The model consists of 2 concentric spherical shells, at a distance of 1500 pc, characterised respectively by expansion velocities of 35 and 164 km s–t, outer radii of 1.3 x 10^{17} and 7.2 x 10^{17} cm, mass- loss rates of about 10^{-4} and 10^{-3} $M_\odot$ yr^{-1}, and

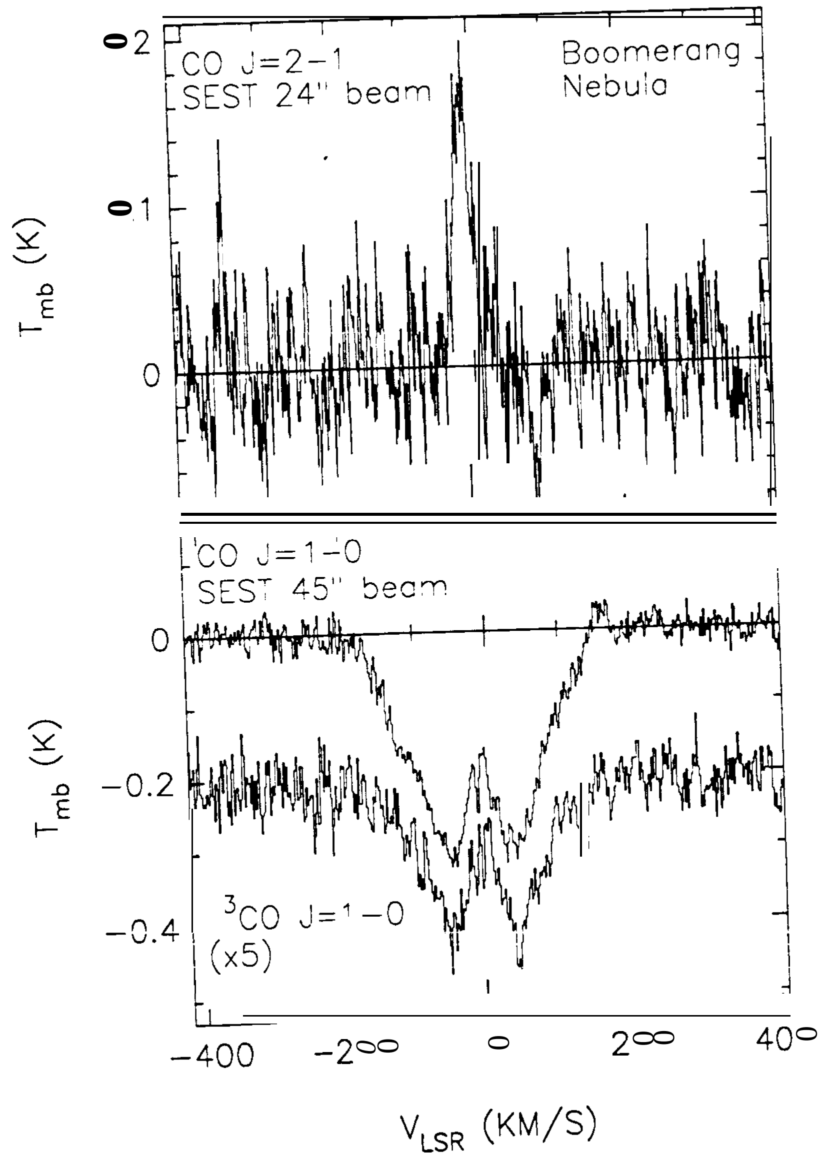
CO J=2−1
SEST 24'' beam
Boomerang
Nebula
CO J=1−0
SEST 45'' beam
3CO J=1−0
(x5)
T_{mb} (K)
V_{LSR} (KM/S)
−400
0

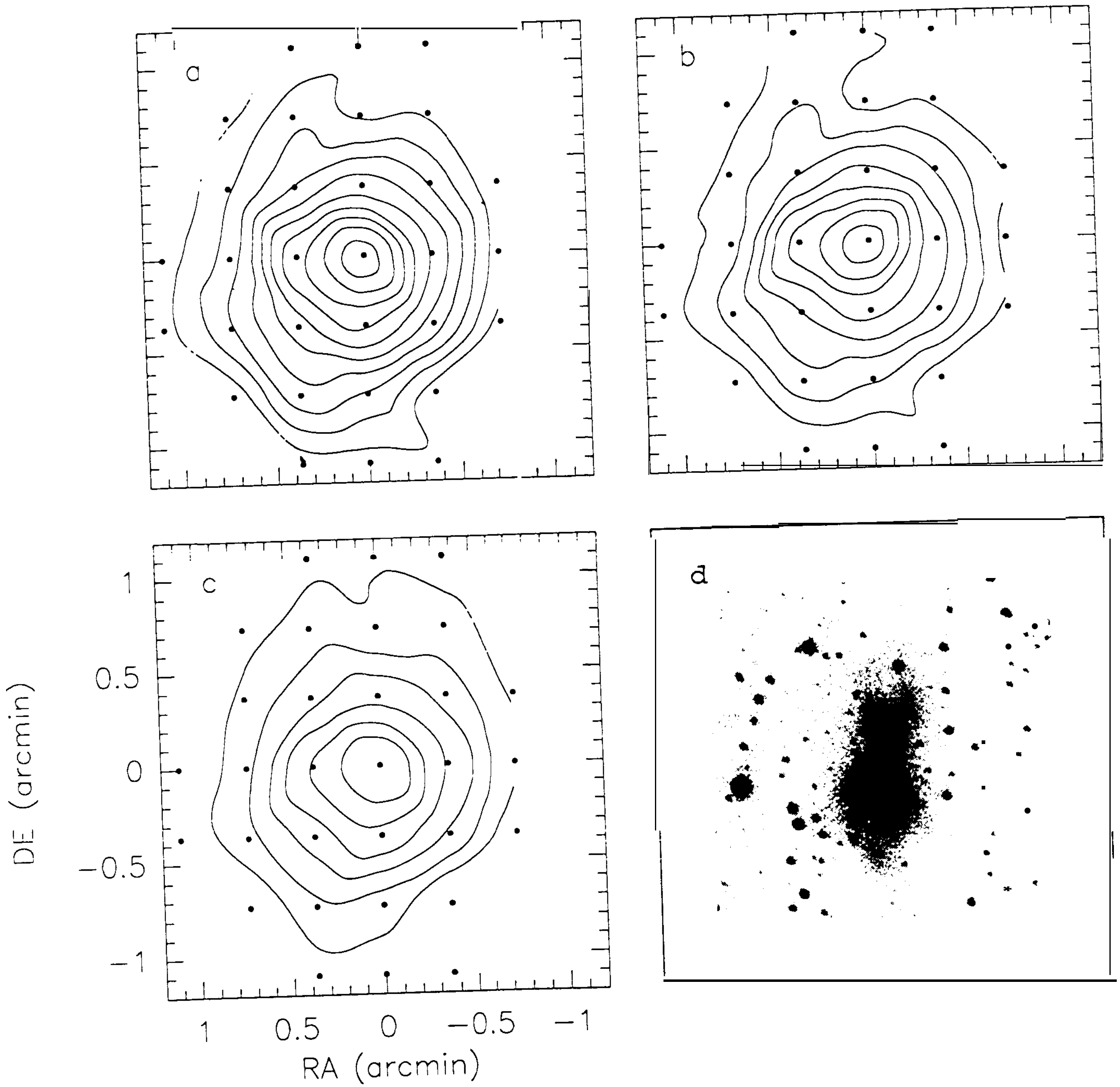
a
b
c
d
DE (arcmin)
1
0.5
0
−0.5
−1
RA (arcmin)
1
0.5
0
−0.5
−1

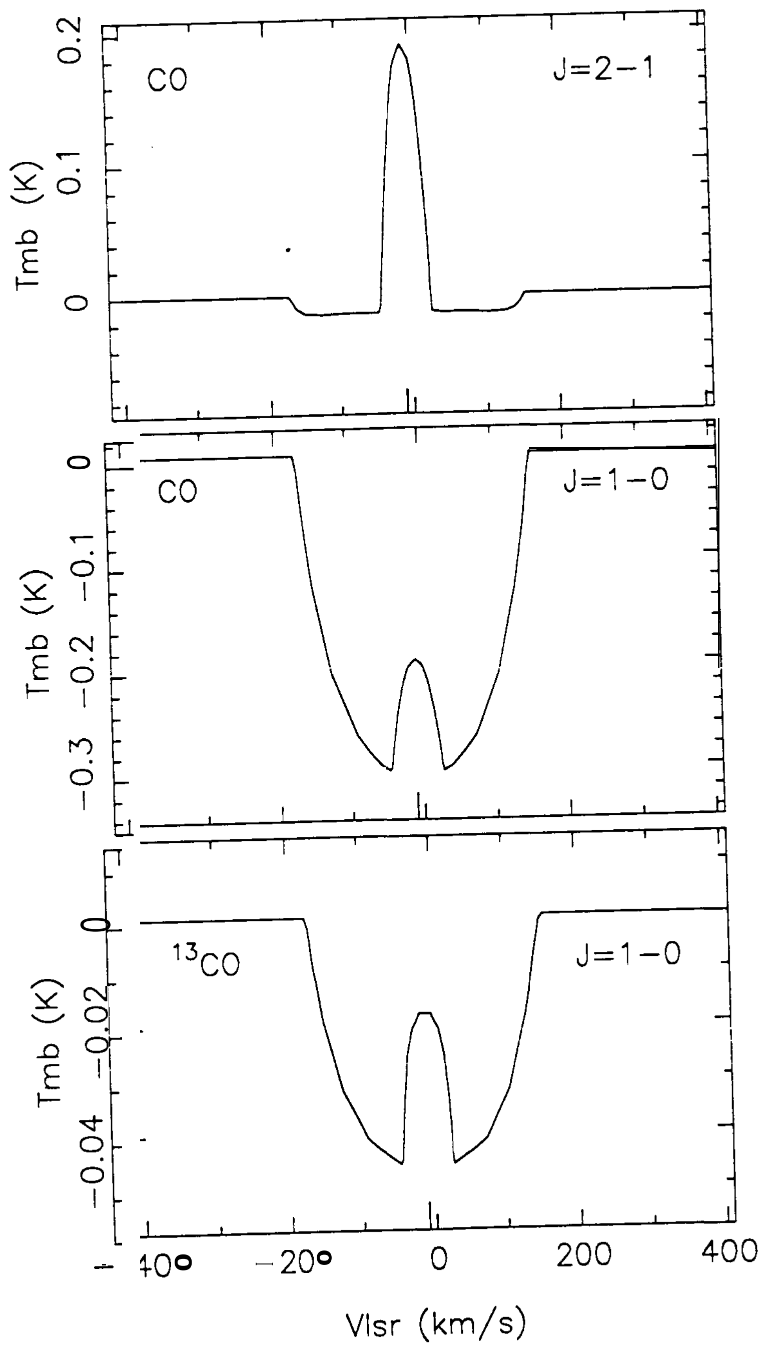

CO
J=2−1
CO
J=1−0
13CO
J=1−0
Tmb (K)
0.2
0.1
0
−0.1
−0.2
−0.3
−0.02
−0.04
−400
−200
200
400
Vlsr (km/s)

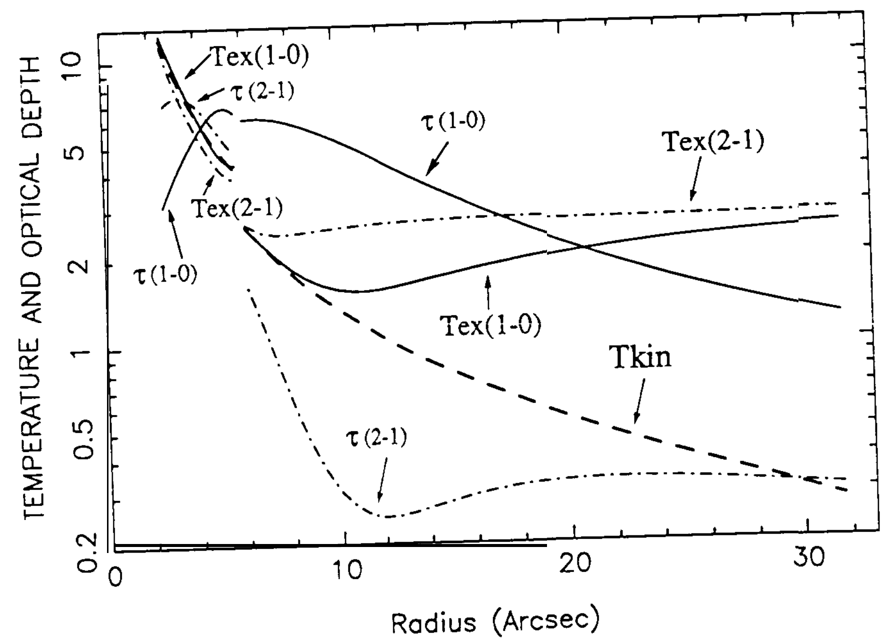
TEMPERATURE AND OPTICAL DEPTH
Radius (Arcsec)
0.2
0.5
1
2
5
10
0
10
20
30
Tex(1-0)
τ (2-1)
τ (1-0)
Tex(2-1)
τ (1-0)
Tex(2-1)
Tex(1-0)
Tkin
τ (2-1)